Journal of Magnetism and Magnetic Materials 382 (2015) 1–6

Contents lists available at ScienceDirect

Journal of Magnetism and Magnetic Materials

journal homepage: www.elsevier.com/locate/jmmm

Structural evolution and enhanced magnetization of $Bi_{1-x}Pr_xFeO_3$

Jing Zhang [a,b], Yu-Jie Wu [c,b], Xiao-Jia Chen [d,*]

[a] School of Mathematics and Physics, Beijing Institute of Technology, Zhuhai 519088, China
[b] Department of Physics, South China University of Technology, Guangzhou 510640, China
[c] School of Physics and Electronic Engineering, Guangzhou University, Guangzhou 510006, China
[d] Center for High Pressure Science and Technology Advanced Research, Shanghai 201203, China

ARTICLE INFO

Article history:
Received 30 October 2014
Received in revised form
11 January 2015
Accepted 23 January 2015
Available online 26 January 2015

Keywords:
Multiferroic materials
Structural transition
Magnetic property

ABSTRACT

The structural, ferroelectric, vibrational, and magnetic properties of polycrystalline $Bi_{1-x}Pr_xFeO_3$ ($0 \le x \le 0.50$) powders are investigated by the measurements of X-ray diffraction, X-ray photoelectron spectroscopy, Raman scattering spectroscopy, and magnetization at room temperature. Our results reveal that the rare-earth ion Pr substitution at Bi site causes the structural transformations from rhombohedral *R*3*c* phase to orthorhombic *Pbam* phase at $x \approx 0.15$, and then to orthorhombic *Pnma* phase at higher Pr concentration $x \approx 0.25$, accompanying the ferroelectric–antiferroelectric–paraelectric phase transition. Measurements of magnetic properties confirm that Pr substitution can improve the magnetization of $BiFeO_3$ before approaching the first phase transition. We find that an inverse behavior occurs after passing a maximum across the antiferroelectric–paraelectric phase boundary. We also obtain the unique switching behavior in low magnetic field of $Bi_{0.5}Pr_{0.5}FeO_3$ from the field dependence on magnetization, indicating the existence of the antiferromagnetic ordering.

1. Introduction

In recent years, much attention has been paid to the multiferroic materials which display ferroelectricity, ferromagnetism and/or ferroelasticity simultaneously in a single phase [1], owing to their interesting physical phenomena and considerable potential applications in data storage, sensors and actuators, etc. [2–4]. Among these multiferroics materials, bismuth ferrite ($BiFeO_3$) has been extensively explored because of its ferroelectric transition temperature and antiferromagnetic Néel temperature well above the room temperature [5]. $BiFeO_3$ is a rhombohedrally distorted perovskite with space group *R*3*c* (Ref. [6]) and described as an $a^-a^-a^-$ tilt system in which the FeO_6 octahedra rotate around the $\langle 111\rangle_p$ (where p=pseudocubic) direction [7]. However, the local short-range order of $BiFeO_3$ is *G*-type antiferromagnet with a cycloid spatial spin modulation with a period of 62 nm [8]. In this way, each Fe^{3+} spin is surrounded by six antiparallel spins on the nearest Fe neighbors, preventing the observations of noticeable magnetization [9]. On the other hand, the ferroelectricity of $BiFeO_3$ mainly arises from the Bi site atoms [10] which are not located exactly in the middle between the FeO_6 octahedra as a result of the off-center displacement of Bi^{3+} caused by the presence of 6*s* lone pair electrons [11]. In the Bi-based perovskites, the $6s^2$ electrons of Bi^{3+} hybridize with 2*s* and 2*p* of oxygen to form a space-filling localized lobe, which in turn pushes away its neighboring atoms causing a structural distortion [12]. Both effects help to induce ferroelectricity [11,13]. However, it is always difficult to obtain the spontaneous polarization in bulk $BiFeO_3$ or the good saturated hysteresis loop *P*–*E* due to the large leakage current [14].

Many attempts have been made to improve the ferroelectricity and magnetization in $BiFeO_3$. The effective way to improve the magnetic properties is to offer internal [14–30] and/or external [31–34] stresses to $BiFeO_3$. The internal stress provided by the substitution of rare-earth cations at the Bi-site of $BiFeO_3$ can effectively modulate the crystal structure parameters and destroy the cycloid spin structure. The effect of cation substitution can lead to the release the locked magnetic moment and the improvement of magnetization [14–22]. However, some researchers considered that the enhanced magnetization can be partly attributed to the existence of Fe^{2+} ion and/or the impurity phase $Bi_{25}FeO_{39}$ [23,24]. Therefore, there is still a debate of the mechanism of the magnetization improvement. For ferroelectric property, the recent investigations on $Bi_{1-x}Re_xFeO_3$ (Re=La [25], Nd [26,27], Sm [28,29], Gd [30]) systems showed that an alike $PbZrO_3$ orthorhombic *Pbam* structure with antiferroelectricity appeared stably between the rhombohedral *R*3*c* and the orthorhombic *Pnma* phase boundaries. It is found that the obtained range of *Pbam* phase in $Bi_{1-x}Re_xFeO_3$ compounds is very narrow due to the smaller ionic radius of Re^{3+} ion substitutes [26,27,30]. Consequently, it can be assumed that the substitution of Pr^{3+} with larger ionic radius (1.32 Å) at Bi-site

* Corresponding author.
E-mail address: xjchen@hpstar.ac.cn (X.-J. Chen).

http://dx.doi.org/10.1016/j.jmmm.2015.01.061
0304-8853/

will display a wider and more stable configuration of *Pbam* phase. However, there were very few papers focusing on the Pr-doped $BiFeO_3$ system [35–37], and none of them discovered the $PbZrO_3$-like orthorhombic *Pbam* phase. Kumar et al. [35] found that the structure transition from rhombohedral *R3c* to triclinic *P1* in $Bi_{1-x}Pr_xFeO_3$ ($0 \le x \le 0.15$). Moreover, all reports [35–37] showed that both the polarization and dielectric constant increase with increasing Pr substituted concentration *x*. It was attributed to the reduction of oxygen vacancies resulting from the substitution of high valence Pr^{4+} for Bi^{3+}, and the lattice distortion derived from the difference in ionic radius and electronic structures between Pr and Bi ions [35–37]. However, the simplex influence of structural distortion on the ferroelectric property is still under debate.

In this paper, we aim to exhibit clear images of Pr substituted $BiFeO_3$ compounds within the concentration range of $0 \le x \le 0.5$ through the investigations of the structural, ferroelectric, vibrational, and magnetic properties. The high quality samples enable us to understand better about the relations among the structure, ferroelectricity, and ferromagnetization. We show the evidence for the existence of an antiferroelectric orthorhombic *Pbam* phase between ferroelectric orhombohedral *R3c* and paraelectric orthorhombic *Pnma* phases. There is giant magnetization improvement approaching the polar–antipolar–nonpolar phase transitions.

2. Experimental

$Bi_{1-x}Pr_xFeO_3$ powders were synthesized by a tartaric acid ($C_4H_6O_6$) modified sol–gel technique. Appropriate amounts of Bi $(NO_3)_3 \cdot 5H_2O$, $Pr(NO_3)_3 \cdot 6H_2O$, and $Fe(NO_3)_3 \cdot 9H_2O$, were dissolved in dilute nitric acid, and calculated amounts of tartaric acid were added as a complex agent. The resultant solution was evaporated and dried at 150 °C with continuous stirring to obtain xerogel powders. Then the xerogel powders were ground in an agate mortar and subsequently preheated to 300 °C for 1 h to remove excess hydrocarbons and NO_x impurities. Finally, all samples were further annealed at 600 °C for 2 h. Phase analysis and investigation of the crystal structure were performed by x-ray diffraction (XRD) technique using a Bruker D8 ADVANCE diffractometer with Cu *Kα* radiation. X-ray photoelectron spectroscopy (XPS) (ESCA Kratos AUD) was used to determine the oxidation states of Fe and Pr ions in the $Bi_{1-x}Pr_xFeO_3$ powders. Raman spectra were recorded in backscattering geometry with a LABRAM Jobin–Yvon spectrometer using a He–Ne laser of wavelength 633 nm. Magnetic properties were measured by using the Physical Properties Measurement System (PPMS, Quantum Design) at room temperature.

3. Results and discussion

All XRD patterns were refined well using the Fullprof Rietvled method. Fig. 1 shows the results of selected XRD measurements of $Bi_{1-x}Pr_xFeO_3$ ($x=0.04$, 0.20, 0.50) powders. There is no trace of routine impurity phases such as $Bi_2Fe_4O_9$, $Bi_{25}FeO_{40}$ and/or Pr_6O_{11} in all samples, indicating a balanced proportion between Bi/Pr and Fe. $BiFeO_3$ is well defined as rhombohedral *R3c* symmetry at room temperature, and the unit cell parameters are $a=b=5.57036$ Å and $c=13.84314$ Å.

For Pr-substituted concentration $x \le 0.125$, the XRD patterns can be well refined using a polar rhombohedral *R3c* model as shown in Fig. 1(a). There are some new diffraction peaks appearing around $2\theta \approx 17.7°$, 28.9° and 33.0°at $x=0.15$, which indicate a structure transition. A thorough analysis of the diffraction spectra indicated the second phase can be well described using the

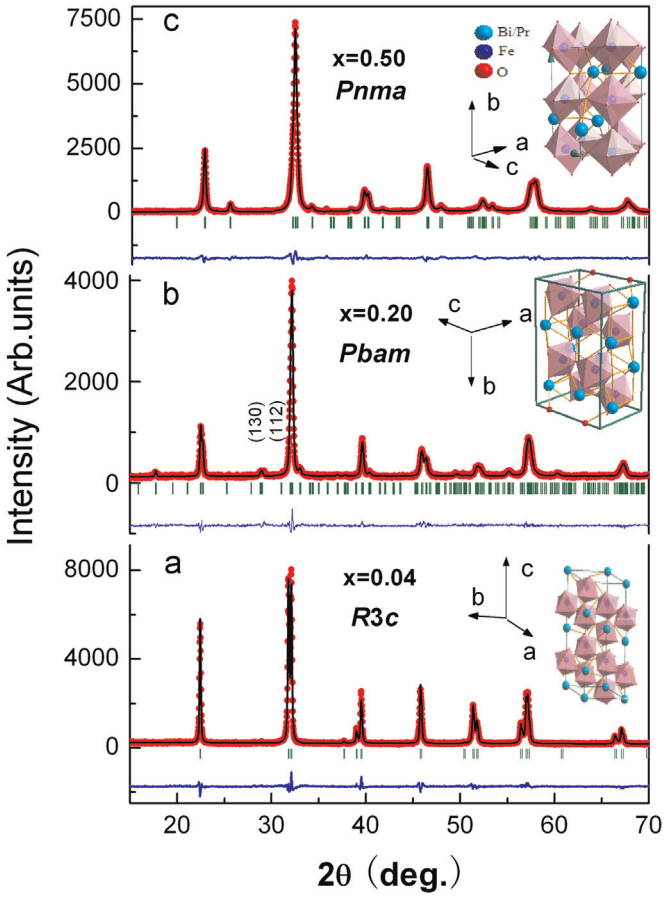

Fig. 1. Observed, calculated, and difference XRD patterns for (a) $Bi_{0.96}Pr_{0.04}FeO_3$, (b) $Bi_{0.80}Pr_{0.20}FeO_3$, and (c) $Bi_{0.50}Pr_{0.50}FeO_3$ samples at room temperature. The refined space groups are given. The insets show schematic representations of the corresponding structures (*R3c*, *Pbam*, and *Pnma*, respectively).

$PbZrO_3$-like orthorhombic *Pbam* symmetry structure which is characteristic of $\sqrt{2}a \times 2\sqrt{2}a \times 2a$ (where *a* is the pseudocubic lattice parameter, $a \sim 4$ Å) supercell [38]. The space group *Pbam* combines antiphase rotations of the BO_6 octahedra described by $a^-a^-c^0$ tilting system with antipolar displacements of Pb ions along the $\langle 110 \rangle_p$ (where *p* is pseudocubic) axis [26,38]. The fit at $0.15 \le x \le 0.25$ with *Pbam* was very satisfactory, in which we replaced the Pb ions with Bi and Pr ions in the $PbZrO_3$ space group model. This confirms the phase transformation observed around $x=0.15$ is from rhombohedral *R3c* symmetry to orthorhombic *Pbam* phase accompanying a ferroelectric–antiferroelectric phase transition. With increasing the Pr concentration *x*, the characteristic peaks (110), (130) and (112) of the orthorhombic *Pbam* phase disappeared above $x=0.25$, while the characteristic diffraction peak around 25° of *Pnma* appeared. It suggests another structure transformation from *Pbam* to *Pnma*. The selected $Bi_{0.50}Pr_{0.50}FeO_3$ sample is well refined using a *Pnma* cell with $a=5.57675$ Å, $b=7.814$ Å, and $c=5.49668$ Å. The space group *Pnma* is a centrosymmetry structure with a paraelectric ordering, and has an $a^-a^-c^+$ tilting system with $\sqrt{2}a \times 2a \times \sqrt{2}a$ supercell [39], which implied that the second structure transition accompanied the antiferroelectric–paraelectric phase transformation.

Notably, the existence range of *Pbam* phase in $Bi_{1-x}Pr_xFeO_3$ ($0.15 \le x \le 0.25$) powders is broader than that in $Bi_{1-x}Nd_xFeO_3$ and $Bi_{1-x}Sm_xFeO_3$ [26,27,30]. There was even no single *Pbam* phase existed particularly in $Bi_{1-x}Gd_xFeO_3$ and $Bi_{1-x}Dy_xFeO_3$ samples [23,30]. This is attributed to the radius of Pr^{3+} ion (1.32 Å) is larger than Nd^{3+} (1.31 Å), Sm^{3+} (1.28 Å), Gd^{3+} (1.27 Å), and Dy^{3+} (1.24 Å) ions. Also it is the nearest one to the radius of Bi^{3+} ion.

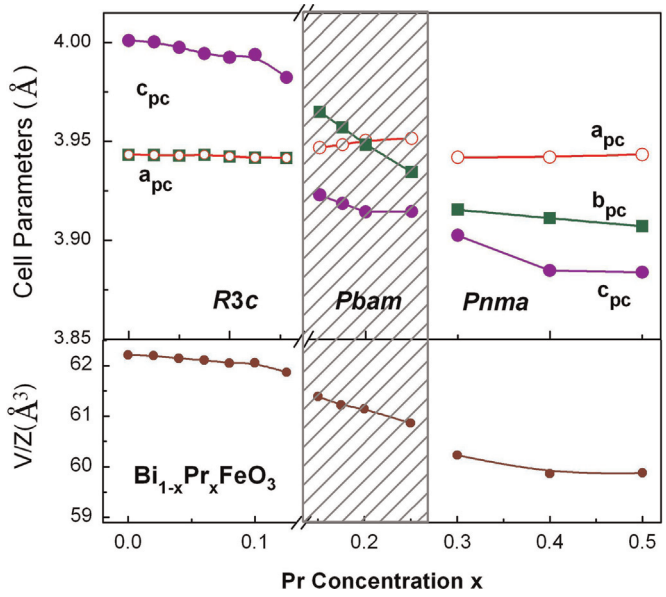

Fig. 2. The substitution x dependence of the unit-cell volume V divided by the number of formula unites per unit cell Z, the normalized lattices parameters of $Bi_{1-x}Pr_xFeO_3$ ($0 \le x \le 0.50$). The cell parameters are described in a pseudocubic cell $a_{pc} = a/\sqrt{2}$, and $c_{pc} = c/2\sqrt{3}$ for the $R3c$ phase, $a_{pc} = a/\sqrt{2}$, $b_{pc} = b/2\sqrt{2}$ and $c_{pc} = c/2$ for the *Pbam* phase, $a_{pc} = a/\sqrt{2}$, $b_{pc} = b/2$, and $c_{pc} = c/\sqrt{2}$ for the *Pnma* phase.

The size of the dopant has significant impact on the structural distortion. With equivalent substituted concentration, the smaller Re^{3+} ion substitution will cause larger lattice distortion, which is attributed to a chemical-like pressure effect caused by the smaller radii of the isovalent Re ions. It has been reported that the *Pbam* phase was also found in pure $BiFeO_3$ by an external hydrostatic pressure during decompression [40].

The *Pbam* phase of $Bi_{1-x}A_xFeO_3$ (A=La,Nd,Sm) has been identified as the antiferroelectric $PbZrO_3$ structure [26,27,30,41,42]. The structural distortions within the cell can be considered as antipolar Pb displacements and antiphase rotations of the O octahedral described by an $a^-a^-c^0$ tilting system [43]. The combination of these two structural distortions gives rise to anti-ferroelectricity. The same *Pbam* structure of our $Bi_{1-x}Pr_xFeO_3$ ($0.15 \le x \le 0.25$) samples accounts for its anti-ferroelectric characteristic as observed in similar systems.

In order to analyze the structural distortion quantitatively, we summarize the evolutions in the cell parameters and unit cell volume with Pr-doped concentration x in Fig. 2 expressed by a pseudo-cubic cell. As can be seen, the volume decreases with increasing Pr-substituted concentration x and shows two abrupt changes around $x=0.15$ and 0.3. This is due to lattice distortion resulted from the difference ionic radii between Pr^{3+} (1.32 Å) and Bi^{3+} (1.36 Å), and the abrupt changes are evidences of the phase transitions. Additionally, the slight reduction of a_{pc} and c_{pc} is observed, with increasing x at the low Pr-doped concentration region. However, all the axes show clearly abrupt evolution in the ranges of $0.125 \le x \le 0.15$ and $0.25 \le x \le 0.3$. It can be explained by the occurrence of the structural transformations from rhombohedral $R3c$ symmetry to orthorhombic *Pbam* phase, and finally to another orthorhombic *Pnma* phase. In the *Pbam* symmetry, the a_{pc} lattice parameter begins to increase and, conversely, b_{pc} decreases quickly. Nevertheless, the c_{pc} axis continues to decrease. The a_{pc}, b_{pc}, and c_{pc} cell parameters keep the same variation trends at the higher substitution concentration $x=0.3$–0.5, accompanying a sudden change between $x=0.25$ and 0.30. Generally speaking, these abnormal phenomena at the phase boundary can be ascribed to the largest lattice distortion and the drastic competition between two phases resulting from the Pr substitution in the Bi-site.

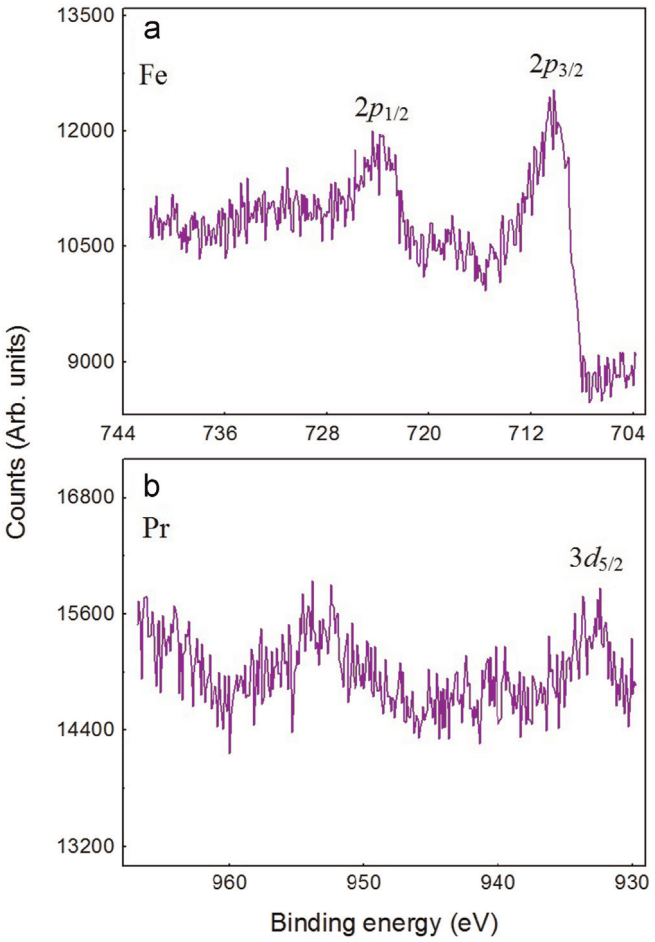

Fig. 3. X-ray photoelectron spectra of the Fe 2p line (a) and Pr 3d line (b) for $Bi_{0.92}Pr_{0.08}FeO_3$ compound.

In order to ensure the oxidation states of Fe and Pr ions in the $Bi_{1-x}Pr_xFeO_3$ powders, we carried out the X-ray photoemission spectroscopy (XPS) measurement, as shown in Fig. 3. It is well known that Fe 2p core level splits into $2p_{1/2}$ and $2p_{3/2}$ components. The binding energy of Fe $2p_{3/2}$ is expected to be 710.7 eV for the Fe^{3+} while 709.3 eV for the Fe^{2+} [44]. From the XPS spectrum, we observe that the peak of Fe $2p_{3/2}$ is exactly located at 710.8 eV. Moreover, its satellite peak is closer to the side of the Fe $2p_{1/2}$ peak. These two characteristics indicate that the Fe valence in the composite film should be Fe^{3+} and there are no Fe^{2+} ions. The result substantiates that the replacement of some volatile Bi^{3+} ions with nonvolatile Pr^{3+} ions is helpful to prevent the formation of oxygen ion vacancies and suppress valence fluctuation of Fe ions from the +3 to the +2 state in $BiFeO_3$ [45]. The core level XPS spectrum for Pr is shown in Fig. 3(b). The binding energy of Pr $3d_{5/2}$ state is 933.2 eV and 935.3 eV in Pr_2O_3 (Pr^{3+}) and PrO_2 (Pr^{4+}) [46]. The binding energy of the Pr $3d_{5/2}$ state is 933.1 eV in our Pr-doped $BiFeO_3$ samples, indicating the ionic state of Pr is close to the ionic state of the element in Pr_2O_3 [47]. It may be noted that the Pr ionic state is thought of a mixed states of +3 and +4 in the previous works [35–37]. This is because they use Pr_6O_{11} as the dopant oxide, which is known that the oxidation state of Pr ion is a mixture of +3 and +4 in oxides. Moreover, all the ceramic samples in the previous reports are not single phase, existing $Bi_{25}FeO_{39}$ [35], $Bi_2Fe_4O_7$ and/or $Bi_{46}Fe_2O_{72}$ [36]. Consequently, the Pr^{3+} ion is more advantageous to form single phase $Bi_{1-x}Pr_xFeO_3$

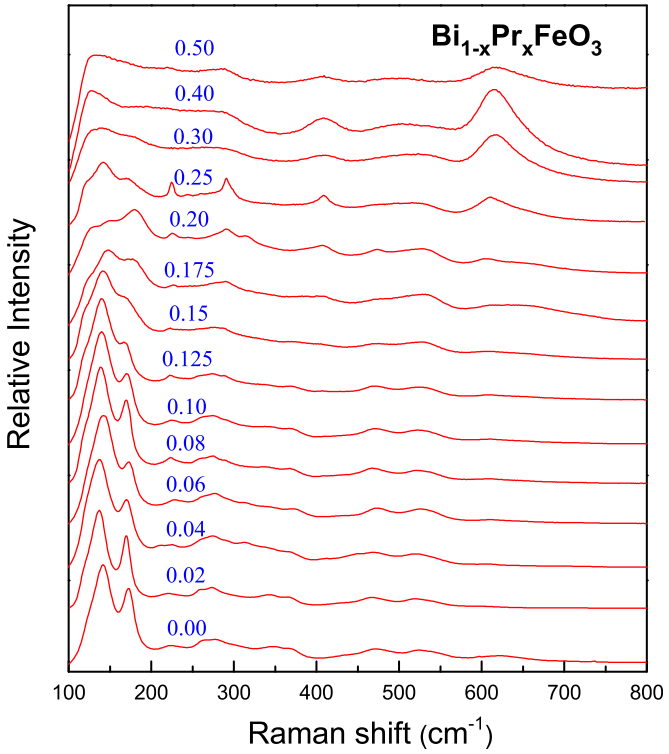

Fig. 4. Raman scattering spectra of $Bi_{1-x}Pr_xFeO_3$ ($0 \le x \le 0.50$) compounds at room temperature.

compositions. Therefore, the increased magnetization observed later cannot yet result from Fe^{2+}.

Raman scattering is a very informative technique to study the local distortion in ABO_3 system. It is sensitive to the changes of atomic displacement, the evolution of Raman modes with increasing Pr content. Unpolarized Raman spectra were carried out for all $Bi_{1-x}Pr_xFeO_3$ ($0 \le x \le 0.5$) powders at room temperature, as shown in Fig. 4. According to group theory, pure $BiFeO_3$ with rhombohedral *R*3*c* structure has 13 Raman active modes, illustrated as $\Gamma = 4A_1 + 9E$ [48], while 24 Raman-active modes are corresponding to the *Pbam* and *Pnma* orthorhombic structure with $\Gamma = 13A_g + 13B_{1g} + 11B_{2g} + 11B_{3g}$ [49] and $\Gamma = 7A_g + 5B_{1g} + 7B_{2g} + 5B_{3g}$ [50], respectively. Just 13 Raman modes obtained in *Pbam* phase, and only 11 modes in *Pnma* phase are observed. The number of unpolarized Raman-active modes is about half of the polarized ones in *Pbam* and *Pnma* orthorhombic structure [51].

In order to understand the relationship between the frequency of Raman modes and the Pr concentration *x*, we fitted the Raman spectra with Lorentzian shapes. Fig. 5 shows the Pr concentration *x* dependence of the frequency of Raman active modes. For pure $BiFeO_3$, there are 13 Raman modes in accordance with previously theoretical results. It is notable that all the modes shift slowly in the low substituted range $0 \le x \le 0.125$, which illustrate the structures are stable and just distort slightly. The peaks located 121, 136, 170, 215, and 260 cm^{-1} in pure $BiFeO_3$ are described as *E*-1, A_1-1, A_1-2, A_1-3, and *E*-2 modes, respectively, which are governed by the relative motion of *A*-site cations against the oxygen octahedrons. They shift slowly to higher frequency with increasing Pr content *x*. This is due to the decrease of the Bi–O bond caused by gradually replacement of Pr^{3+} at Bi-site. As Pr content increases from 0.125 to 0.15, one dramatic shift can be found in the vibrational modes in the region of 200–300 cm^{-1}. Another abrupt change is that a new peak at around 650 cm^{-1} appears at $x = 0.15$. These phenomena are attributed to the larger lattice distortion at the phase transition boundary, resulting from the drastic

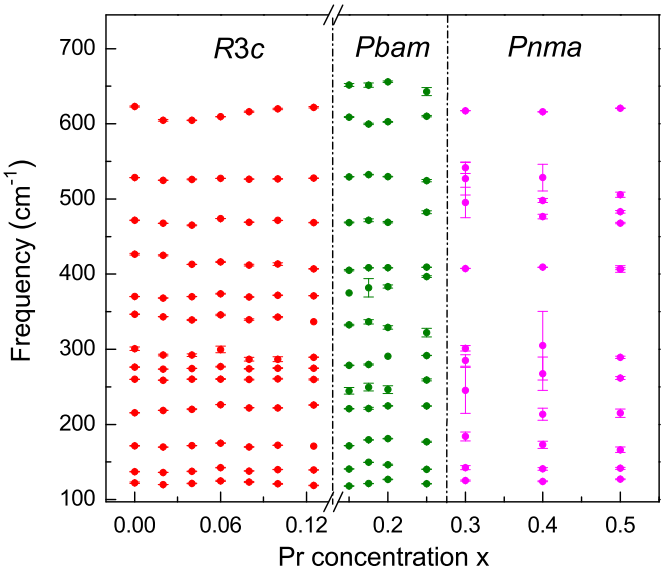

Fig. 5. The Pr substituted concentration *x* dependence of frequency shifts of Raman active modes of $Bi_{1-x}Pr_xFeO_3$ ($0 \le x \le 0.50$) compounds.

competition between the rhombohedral *R*3*c* symmetry and orthorhombic *Pbam* phase. In the Pr concentration range of $0.15 \le x \le 0.25$, the two peaks near 375 and 405 cm^{-1} shift to higher frequency and get closer to each other gradually with increasing concentration *x*. It is striking that the two highest frequency modes, about 609 and 652 cm^{-1}, shift separately at first and then get close. A larger sudden frequency shifts is observed at $x = 0.30$. Between $x = 0.25$ and 0.30, the prominent feature in the Raman spectra is the superposition of the modes around 397 and 409 cm^{-1} and mergence of the modes around 610 and 642 cm^{-1}, respectively. The vibrational mode around 407 cm^{-1} assigned as B_{3g} symmetry, connected with (101) distortion of the FeO_6 octahedral [52], is the intrinsic modes of the orthorhombic *Pnma* phase [53], revealing the occurrence of the *Pbam*–*Pnma* transformation. The phase boundary determined based on Raman scattering technique results is in good agreement with the results from XRD patterns.

Fig. 6 shows the magnetic hysteresis loops of the selected $Bi_{1-x}Pr_xFeO_3$ ($x = 0$, 0.15, 0.4, and 0.5) samples with a maximum applied magnetic field of 8.0 T at room temperature. It is well known that the pure $BiFeO_3$ has a G-type antiferromagnetic

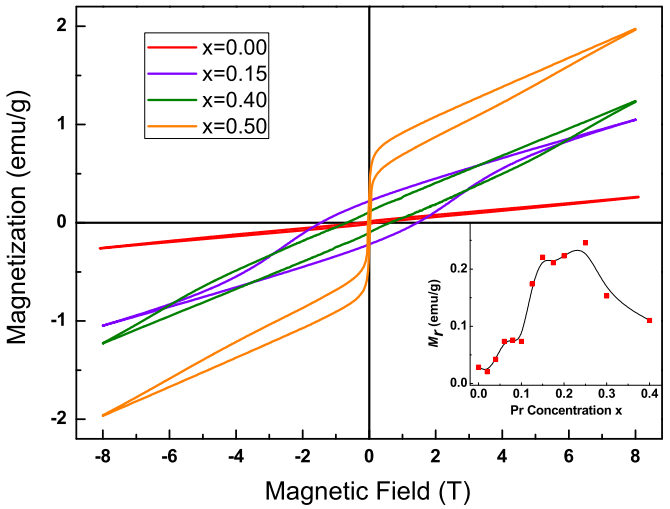

Fig. 6. Room temperature *M*–*H* curves of $Bi_{1-x}Pr_xFeO_3$ ($x = 0.0$, 0.15, 0.4 and 0.5). The inset shows Pr composition *x* dependent remnant magnetization.

ordering with a spatially modulated spiral spin structure, leading to null macroscopic magnetization. However, our $BiFeO_3$ powders show a narrow ferromagnetic hysteresis loop with a remanent magnetization $M_r \approx 0.029$ emu/g. The spontaneous magnetization should result from the uncompensated spin magnetic moments due to the grain size of particles smaller than 62 nm. The obvious openings in the hysteresis loops of $Bi_{1-x}Pr_xFeO_3$ $(0 < x \leq 0.2)$ confirm that the magnetic properties are improved owing to the Pr substitution at the Bi site. The inset of Fig. 6 presents the measured magnetization value (M_r) as the function of the Pr concentration x. For $x \leq 0.125$, the remanent magnetization of $Bi_{1-x}Pr_xFeO_3$ samples increases gradually with increasing Pr substituted concentration x. A dramatic enhancement in the remanent magnetization appears in the range of $x=0.125$–0.15, accompanied with the structural crossover from *R3c* phase to *Pbam* symmetry. In the antipolar *Pbam* phase ($0.15 \leq x < 0.3$), the M_r values are very large, which is several times larger than those obtained for the pure $BiFeO_3$. According to the neutron diffraction technique, the enhancement of magnetization could be attributed to the increasing periodicity of spiral spin structure suppressed by Pr substitution, releasing partially latent magnetic moments locked within the cycloid spin structure [54,55]. The Pr substitution can only suppress but cannot destroy the spin cycloid structure completely as the substituted concentration of Pr is below 0.25, and results in a limited increase of the magnetic properties. However, with further increasing x ($x \geq 0.3$), the M_r decreases quickly after passing a maximum value 0.246 emu/g at $x=0.25$. It means that the spiral spin structure is destroyed completely at $x=0.25$. The decrease of magnetization for $x \geq 0.3$ is believed to happen due to further decrease in the extent of canting of spin structure, allowing a more perfect antiferromagnetic order [19,56].

It is more interesting that the magnetic hysteresis loop of $x=0.50$ shows a metamagnetic behavior at low applied field as shown in Fig. 6. This is so called 'switching behavior' found in Y doped $BiFeO_3$ system at low and room temperature [17,57]. This is a distinctive character of applied field induced alignment of spins in an antiferromagnetic order system opening the hysteresis loop. This phenomenon confirms the perfect antiferromagnetic structure existing within the orthorhombic *Pnma* phase of our $Bi_{1-x}Pr_xFeO_3$ powder system. The switching behavior is a special observation at room temperature for the multiferroic classification, and makes it probable candidate for obtaining better magnetoelectric coupling. However, this quite fascinating magnetic behavior of multiferroic materials is required to be further researched on both macroscopic and microscopic horizons.

4. Conclusions

We have successfully synthesized the single phase $Bi_{1-x}Pr_xFeO_3$ $(0 \leq x \leq 0.5)$ powders by the modified sol–gel method. Pr substitution at Bi-site of $BiFeO_3$ has caused the compositional-driven structural transformations from rhombohedral *R3c* phase to orthorhombic *Pbam* phase in the region of $x=0.125$–0.15, then into another orthorhombic *Pnma* phase at $x \approx 0.30$. The structural crossovers were also confirmed by the abrupt evolution of the cell parameters and active vibrational modes at the phase boundaries. These structural transitions brought about an appearance of antiferroelectric ordering in the $PbZrO_3$-like *Pbam* symmetry ($0.15 \leq x \leq 0.25$) between the ferroelectric *R3c* phase ($x \leq 0.125$) and paraelectric *Pnma* phase ($x > 0.25$). We observed the magnetization enhanced gradually with increasing the Pr concentration resulting from the spiral spin magnetic moments suppressed by Pr substituted in initial *R3c* phase. The dramatic increases at the phase transitional edges are attributed to the complete destruction of the spiral spin structure. Interestingly, the magnetization decreased quickly with further increase of Pr doped content after passing the maximum M_r value at $x=0.25$. In fact, the suppressed helical spin arrangement was broken absolutely at the antipolar–nonpolar phase transition, and changed into well unparallel antiferromagnetic ordering. Moreover, the unique switching behavior in low magnetic field is the most interesting observation of the magnetic field dependence of magnetization of $Bi_{0.5}Pr_{0.5}FeO_3$, which is attributed to the perfect antiferromagnetic ordering for $x=0.5$. We expect such a behavior would provide a new possible candidate for obtaining better magnetoelectric coupling.

Acknowledgments

This work was supported by the Cultivation Fund of the Key Scientific and Technical Innovation Project, Ministry of Education of China (No. 708070) and the National Natural Science Foundation of China (Nos. 10874046 and 11104081).

References

[1] G. Catalan, J.F. Scott, Adv. Mater. 21 (2009) 2463.
[2] N.A. Spaldin, M. Fiebig, Science 309 (2005) 391.
[3] Y. Tokura, Science 312 (2005) 1481.
[4] M. Bibes, A. Barthelemy, Nat. Mater. 7 (2008) 425.
[5] R. Haumont, I.A. Kornev, S. Lisenkov, L. Bellaiche, J. Kreisel, B. Dkhil, Phys. Rev. B 78 (2008) 134108.
[6] J.M. Moreau, C. Michel, R. Gerson, W.J. James, J. Phys. Chem. Solids 32 (1971) 1315.
[7] C. Michel, J.M. Moreau, G.D. Achenbach, R. Gerson, W.J. James, Solid State Commun. 7 (1969) 701.
[8] I. Sosnowska, T. Peterlin-Neumaier, E. Steichele, J. Phys. C 15 (1982) 4835.
[9] I. Dzyaloshinsky, J. Phys. Chem. Solids 4 (1958) 241.
[10] C. Ederer, N.A. Spaldin, Phys. Rev. Lett. 95 (2005) 257601.
[11] N.A. Hill, Annu. Rev. Mater. Res. 32 (2002) 1.
[12] P. Ravindran, R. Vidya, A. Kjekshus, H. Fjellvåg, O. Eriksson, Phys. Rev. B 74 (2006) 224412.
[13] R. Seshadri, N.A. Hill, Chem. Mater. 13 (2001) 2892.
[14] X.Q. Zhang, Y. Sui, X.J. Wang, Y. Wang, Z. Wang, J. Alloy. Compd. 507 (2010) 157.
[15] Y.J. Wu, X.K. Chen, J. Zhang, X.J. Chen, J. Appl. Phys. 111 (2012) 053927.
[16] X.K. Chen, Y.J. Wu, J. Zhang, X.J. Chen, Sci. China: Phys. Mech. Astron. 55 (2012) 404.
[17] Y.J. Wu, X.K. Chen, J. Zhang, X.J. Chen, J. Magn. Magn. Mater. 324 (2011) 1348.
[18] Y.J. Wu, X.K. Chen, J. Zhang, X.J. Chen, Physica B 411 (2012) 106.
[19] Y.J. Wu, J. Zhang, X.K. Chen, X.J. Chen, Solid State Commun. 151 (2011) 1936.
[20] J. Zhang, Y.J. Wu, X.K. Chen, X.J. Chen, J. Phys. Chem. Solids 74 (2013) 849.
[21] Y.N. Zheng, Y.J. Wu, Z.X. Qin, X.J. Chen, Chin. J. Chem. Phys. 26 (2013) 157.
[22] V.R. Palkar, D.C. Kundaliya, S.K. Malik, S. Bhattacharya, Phys. Rev. B 69 (2004) 212102.
[23] V.A. Khomchenko, D.V. Karpinsky, A.L. Kholkin, N.A. Sobolev, G.N. Kakazei, J. P. Araujo, I.O. Troyanchuk, B.F. Costa, J.A. Paixão, J. Appl. Phys. 108 (2010) 074109.
[24] F.Z. Qian, J.S. Jiang, S.Z. Guo., D.M. Jiang, W.G. Zhang, J. Appl. Phys. 106 (2009) 084312.
[25] I.O. Troyanchuk, D.V. Karprinsky, M.V. Bushinsky, V.A. Khomchenko, G. N. Kakazei, J.P. Araujo, M. Tovar, V. Sikolenko, V. Efimov, A.L. Kholkin, Phys. Rev. B 83 (2011) 054109.
[26] S. Karimi, I.M. Reaney, I. Levin, I. Sterianou, Appl. Phys. Lett. 94 (2009) 112903.
[27] I. Levin, S. Karimi, V. Provenzano, C.L. Dennis, H. Wu, T.P. Comyn, T. J. Stevenson, R.I. Smith, I.M. Reaney, Phys. Rev. B 81 (2010) 020103(R).
[28] S. Fujino, M. Murakami, V. Anbusathaiah, S.-H. Lim, V. Nagarajan, C.J. Fennie, M. Wuttig, L.S. Riba, I. Takeuchi, Appl. Phys. Lett. 92 (2008) 202904.
[29] V.A. Khomchenko, J.A. Paixão, V.V. Shvartsman, P. Borisov, W. Kleemann, D. V. Karpinsky, A.L. Kholkin, Scr. Meter 62 (2010) 238.
[30] S. Karimi, I.M. Reaney, Y. Han, J. Pokorny, I. Sterianou, J. Mater. Sci. 44 (2009) 5102.
[31] O.E. González-Vázquez, J. Íñiguez, Phys. Rev. B 79 (2009) 064102.
[32] M. Ramazanoglu, W. Ratcliff II, H.T. Yi, A.A. Sirenko, S.-W. Cheong, V. Kiryukhin, Phys. Rev. Lett. 107 (2011) 067203.
[33] Y.J. Wu, Z.X. Qin, X.K. Chen, J. Zhang, J. Liu, Z.G. Wu, X.J. Chen, J. Phys.: Condens. Matter 25 (2013) 365401.
[34] Y.J. Wu, X.K. Chen, J. Zhang, J. Liu, W.S. Xiao, Z.G. Wu, X.J. Chen, J. Appl. Phys. 114 (2013) 154110.
[35] N. Kumar, N. Panwar, B. Gahtori, N. Singh, H. Kishan, V.P. Awana, J. Alloy. Compd. 501 (2010) L29.

[36] P. Uniyal, K.L. Yadav, J. Phys.: Condens. Matter 21 (2009) 405901.
[37] B.F. Yu, M.Y. Li, Z.Q. Hu, L. Pei, D.Y. Guo, X.Z. Zhao, S.X. Dong, Appl. Phys. Lett. 93 (2008) 182909.
[38] A.M. Glazer, K. Roleder, J. Dec, Acta Crystallogr. Sect. B: Struct. Sci. 49 (1993) 846.
[39] M. Marezio, J.P. Remeika, P.D. Dernier, Acta Crystallogr. Sect. B: Struct. Sci. 26 (1970) 2008.
[40] A.A. Belik, H. Yusa, N. Hirao, Y. Ohishi, E. Takayama-Muromachi, Chem. Mater. 21 (2009) 3400.
[41] C.-J. Cheng, D. Kan, S.-H. Lim, W.R. McKenzie, P.R. Munroe, L.G. Salamanca-Riba, R.L. Withers, I. Takeuchi, V. Nagarajan, Phys. Rev. B 80 (2009) 014109.
[42] S.B. Emery, C.-J. Cheng, D. Kan, F.J. Rueckert, S.P. Alpay, V. Nagarajan, I. Takeuchi, B.O. Wells, Appl. Phys. Lett. 97 (2010) 152902.
[43] E. Sawaguchi, H. Maniwa, S. Hoshino, Phys. Rev. B 83 (1951) 1078.
[44] T. Schedel-Niedrig, W. Weiss, R. Schlögl, Phys. Rev. B 52 (1995) 17449.
[45] G.L. Yuan, S.W. Or, Appl. Phys. Lett. 88 (2006) 062905.
[46] D.D. Sarma, C.N.R. Rao, J. Electron Spectrosc. Relat. Phenom. 20 (1980) 25.
[47] S.K. Pandey, R. Bindu, P. Bhatt, S.M. Chaudhari, A.V. Pimpale, Physica B 365 (2005) 47.
[48] R. Haumont, J. Kreisel, P. Bouvier, F. Hippert, Phys. Rev. B 73 (2006) 132101.
[49] D.K. Shukla, R. Kumar, S.K. Sharma, P. Thakur, R.J. Choudhary, S. Mollah, N. B. Brookes, M. Knobel, K.H. Chae, W.K. Choi, J. Phys. D: Appl. Phys. 42 (2009) 125304.
[50] M.N. Iliev, M.V. Abrashev, H.-G. Lee, V.N. Popov, Y.Y. Sun, C. Thomsen, R. L. Meng, C.W. Chu, Phys. Rev. B 57 (1998) 2872.
[51] M. Cazayous, Y. Gallais, A. Sacuto, R. de Sousa, D. Lebeugle, D. Colson, Phys. Rev. Lett. 101 (2008) 037601.
[52] F.A. Mir, M. Ikram, R. Kumar, J. Raman Spectrosc. 42 (2011) 201.
[53] Y. Yang, Y.L. Liu, K. Zhu, L.Y. Zhang, S.Y. Ma, J. Liu, Y.J. Jiang, Chin. Phys. B 19 (2010) 037802.
[54] I. Sosnowska, W. Schäfer, W. Kockelmann, K.H. Andersen, I.O. Troyanchuk, Appl. Phys. A 74 (2002) s1040.
[55] I. Sosnowska, R. Przenioslo, P. Fischer, V.A. Murashov, J. Magn. Magn. Mater. 160 (1996) 384.
[56] I. Sosnowska, M. Loewenhaupt, W.I. David, R.M. Ibberson, Mater. Sci. Forum 683 (1993) 133.
[57] R.K. Mishra, D.K. Pradhan, R.N. Choudhary, A. Banerjee, J. Phys.: Condens. Matter 20 (2008) 045218.